PHYSICAL REVIEW FLUIDS **9**, 084602 (2024)

Response of turbulent energy spectrum and flow structures when vortical motion of a certain scale is suppressed by artificial forcing

Masato Hirota [*]
Department of Mechanical Systems Engineering, Tohoku University, 6-6-01 Aramaki-Aoba, Aoba-ku, Sendai 980–8579, Japan

Seiichiro Izawa
Department of Engineering, University of Toyama, 3190 Gofuku, Toyama 930–8555, Japan

Yu Fukunishi
Institute of Computational Fluid Dynamics, 1-16-5 Hara-machi, Meguro-ku, Tokyo 152–0011, Japan

(Received 4 March 2024; accepted 25 June 2024; published 7 August 2024)

A numerical experiment is conducted to investigate the response of a homogeneous isotropic turbulent field at a statistically equilibrium state when the energy cascade process is abruptly interrupted. Vortex motions of a certain scale in the inertial subrange are extracted using a Fourier bandpass filter and forcibly damped by applying artificial forces to the small regions that are the target vortices. Once the forces are applied, the target vortices immediately disappear from the flow field, which is followed by a slight increase in kinetic energy in the larger scale range and a decrease in the smaller scale range. The decrease in energy in the smaller scale range is likely to be caused by the decrease in the stretching speeds of the vortices of that range. Next, the behaviors of individual vortices whose scales are either four times or twice as large as the target scale are tracked using a method in which each vortex is reconstructed as a group of vortex units. It is found that the vortices that are twice as large as the target vortices show smaller curvatures and longer lifespans in comparison to the case without artificial forces, while no remarkable changes are found for the vortices that are four times larger.

DOI: 10.1103/PhysRevFluids.9.084602

I. INTRODUCTION

Turbulence is a typical nonlinear system with a high degree of freedom. One of the major features of turbulence is an energy cascade, which is a continuous energy transfer from large-scale motions to small-scale motions. Kolmogorov [1] theoretically deduced that the power spectrum of turbulent kinetic energy has a constant slope of $-5/3$ in the region where the vortex scale is much smaller than the energy-containing scale while much larger than the energy-dissipating scale, which is known as K41. The energy flux across the scale is constant in this inertial subrange. After this K41 theory, various models have been proposed under some assumptions to describe the statistical aspect of turbulence [2–4], including Kolmogorov's revised theory known as K62 [5].

Nowadays, due to remarkable progress in computer resources, we can directly access a large turbulence database obtained by direct numerical simulations (DNSs). Analyses of the nonlinear terms of the Navier-Stokes equation in the wave-number space explain that energy is transferred

[*]Contact author: mhirota@mail.uec.jp

from one scale to a smaller scale through triad interactions [6–8]. In addition, turbulence is found to be composed of a number of fine tubular vortices of the energy-dissipative scale, from the visualization of intense vorticity regions through DNSs [9–12]. In high Reynolds number turbulence, these fine tubular vortices form clusters that act as large vortices, and the spatial intermittency of their distribution becomes significant. The sizes of the clusters are of the energy-containing scale range [13–15]. However, it has been shown that the direct contributions of these fine-scale vortices to the whole turbulent motion are significantly small [16,17]. Therefore, it is difficult to understand the physical mechanism of the energy cascade process through direct observations of such fine-scale vortices.

In studies aimed at investigating the role of the vortical structures and their motions in the energy cascade process, filtering techniques have been employed. Goto [18,19] analyzed positional relationships among the vortices of different scales using Fourier low-pass filters and proposed a physical mechanism of the energy cascade phenomenon: a pair of vortices stretch smaller vortices through the strain field around them and then the stretched vortices stretch even smaller vortices, and so on. Leung *et al.* [20] investigated the geometric relationships and mutual interactions among the vortices in the inertial subrange using the Fourier bandpass filter. In the extracted fields, they evaluated the vorticity generation term, which consists of the strain tensor and the vorticity tensor, and found that the energy transfer takes place in association with the vortex stretching caused by the vortices of a 2–4 times larger scale. Doan *et al.* [21] also conducted a similar analysis against the isotropic turbulence of various Reynolds numbers and reached the same conclusion. For quantitative analysis of the geometry of turbulent vortical structures, some attempts to extract individual vortices and represent them as a group of geometric elements have been conducted. Goto *et al.* [22] analyzed vortical structures of isotropic turbulence driven by both isotropic and anisotropic forces and presented a quantitative picture of the hierarchy of multiscale vortices and their generation mechanism by extracting the vortex axes and using them as a geometric model of vortices. Hirota *et al.* [23] investigated the geometric relationships among vortical structures and the vortex stretching mechanism by directly computing the induced velocity fields of the individual vortices in the inertial subrange, which were extracted using the Fourier bandpass filter and reconstructed as groups of discrete vortex segments. Yoneda *et al.* [24] mathematically formulated the energy cascade model in terms of vortex stretching without using the Kolmogorov's hypotheses. Tsuruhashi *et al.* [25] decomposed isotropic turbulence into different scales using the Fourier bandpass filters and extracted vortex tubes from the decomposed fields. They showed the self-similarity and steadiness of the hierarchy of the vortex tubes and confirmed validity of Yoneda *et al.* [24] assumptions.

The time evolution of kinetic energy associated with turbulent vortex motions has also been studied. Meneveau and Lund [26] measured the Lagrangian correlation coefficient between local kinetic energy at large and small scales by tracking fluid particles in an isotropic turbulence. They reported that kinetic energy at a certain scale is transferred to smaller scales with a time delay. Cardesa *et al.* [27] investigated the temporal evolution of the energy flux across the length scales in turbulent flows and reported that the behavior of the energy flux at one scale follows that of twice the scale with a time delay. Additionally, Cardesa *et al.* [28] extracted regions of intense energy density as coherent structures of turbulence and investigated the interactions among the structures of different scales by tracking them. From the evaluation of the coherent structures of two different scales, they found that the structures of a certain scale are likely to appear inside those twice the size and concluded that the energy of the coherent structures of a certain scale is mainly transferred to those that are half the scale. Although these findings suggest that the spatially localized vortical structures play a role in the energy transfer, the detailed process remains unclear to date.

If one can observe individual vortices from the beginning to the end, it may help in understanding the role of hierarchical vortex motions in the energy cascade process. Several algorithms that can track vortices in a turbulent flow have been proposed [29–31]. In general, the lifespan of a vortex of a certain scale is measured using the timescale, termed the eddy turnover time [2]. For instance, Villermaux *et al.* [32] observed the motion of intense tubular vortices in a grid-generated turbulence in a water tank experiment and showed that their lifespans could be scaled by the turnover time of integral-scale vortices, although some variations exist depending on the measurement conditions. The lifespan of coherent structures in an isotropic turbulence is also reported to be in the order of their turnover time [28]. However, it should be noted that the characteristics of the coherent structures, defined as high-energy-density motions, do not necessarily agree with those of ordinary vortices found in a turbulent field.

This paper describes an approach to better understand the role of vortical structures in the energy cascade. The focus of this paper is the inertial subrange. In fully developed turbulent flow, the energy constantly flows from large to small scales and eventually dissipates into thermal energy. If the vortex motions of a certain scale are artificially removed from the flow, the balance in the energy transfer will be broken, which will especially influence the vortices of the neighboring scales. Our intention is to observe the reactions of these vortices and to uncover the general role of vortices in the energy transfer of a turbulent flow.

In this paper, the vortex motions of a certain scale in the inertial subrange are selectively suppressed by adding a volume force, and the influence of the artificially damped vortices on the vortices of other scales is observed in detail by tracking their motions. The individual vortices in the turbulent field are replaced by a group of short cylindrical vortex segments in advance, and the lifespans and geometric shapes of vortices are compared before and after the artificial damping.

II. PROCEDURE OF ANALYSIS

A. Target flow field

The target fully developed isotropic turbulence in a periodic cubic box of length 2π is obtained through a direct numerical simulation. The governing equations are the three-dimensional vorticity transport equations,

$$\frac{\partial \boldsymbol{\omega}}{\partial t} + (\boldsymbol{u} \cdot \nabla)\boldsymbol{\omega} = (\boldsymbol{\omega} \cdot \nabla)\boldsymbol{u} + \nu \nabla^2 \boldsymbol{\omega} + \nabla \times \boldsymbol{f}_1 + \nabla \times \boldsymbol{f}_2, \tag{1}$$

where $\boldsymbol{\omega}$ is the vorticity vector, t is time, $\boldsymbol{u}$ is the velocity vector, and ν is the kinematic viscosity.

$\boldsymbol{f}_1$ is a solenoidal force of a random phase that drives the turbulence. The solenoidal force is chosen to be divergence-free in Fourier space with the condition

$$\boldsymbol{k} \cdot \hat{\boldsymbol{f}}_1 = 0, \tag{2}$$

where $\boldsymbol{k}$ is the wave number and ˆ indicates the value is in the wave-number space. This condition can be satisfied by writing the force in the form

$$\hat{\boldsymbol{f}}_1(\boldsymbol{k}, t) = A_{\text{ran}}(\boldsymbol{k}, t)\boldsymbol{e}_1(\boldsymbol{k}) + B_{\text{ran}}(\boldsymbol{k}, t)\boldsymbol{e}_2(\boldsymbol{k}), \tag{3}$$

where $\boldsymbol{e}_1$ and $\boldsymbol{e}_2$ are unit vectors orthogonal to each other and to $\boldsymbol{k}$. A_{ran} and B_{ran} are complex random numbers chosen to satisfy the relation

$$< A_{\text{ran}} A^*_{\text{ran}} > + < B_{\text{ran}} B^*_{\text{ran}} >= \frac{F(k)}{2\pi |\boldsymbol{k}|^2}, \tag{4}$$

where $*$ indicates complex conjugate. $F(k)$ defines the spectrum of the solenoidal force, which is kept constant in the low wave-number components of $1 \leqslant |\boldsymbol{k}| \leqslant 2$, and otherwise is zero. The detailed description of the solenoidal force, $\boldsymbol{f}_1$, can be found in Alvelius [33].

The magnitude of the driving force is chosen so the product of the maximum wave number of the simulation and the Kolmogorov length is kept greater than 1.0. The energy-damping force, $\boldsymbol{f}_2$, is another forcing term that is used to suppress vortical motions of a certain length scale and will be described later. A pseudospectral method is used for the spatial discretization, and a fourth-order classical Runge-Kutta method is employed for the time integration. The aliasing errors are removed through a phase-shift method. The computational conditions are summarized in Table I.

TABLE I. Computational conditions. N is total number of grids, Δx is the grid width, Δt the time step, and ν the kinematic viscosity.

N	Δx	Δt	ν
512^3	1.23×10^{-2}	2.0×10^{-3}	3.73×10^{-4}

After the flow field reaches a state of equilibrium, the energy-damping force, $\boldsymbol{f}_2$, in Eq. (1) is then activated, and the time series data before and after the activation, $-4 \leqslant t/T \leqslant 4$, are used in the analyses. The time, $t/T = 0$, corresponds to the time when the energy-damping force, $\boldsymbol{f}_2$, is initiated, where T is the large-eddy turnover time. Here, the large eddy corresponds to the size of those eddies in which the energy to drive turbulence is poured in. The temporal evolution of the turbulent Reynolds number based on the Taylor microscale is shown in Fig. 1 and the time-averaged statistical quantities of the turbulent field are summarized in Table II. Figure 2 shows the energy spectrum at $t/T = 0$. To analyze the interactions among vortical structures with different scales in the inertial subrange, the cutoff wave numbers should be large enough compared with the energy-containing range and sufficiently smaller than the Kolmogorov wave number. Additionally, the bandwidth must be the same on a logarithmic scale. In this paper, the bandwidth is set to be log 2 for $k \in [4, 8], [8, 16], [16, 32]$, and $[32, 64]$, which are represented by their center wave numbers, $k_c = 4\sqrt{2}$, $8\sqrt{2}$, $16\sqrt{2}$, and $32\sqrt{2}$. Hence, the disordered vortices with a characteristic diameter, $l_c = \pi/k_c$, are extracted from the flow field. It should be noted that the extracted vortex scale is given by half of the wavelength. Yoshida *et al.* [34] reported that the high wave-number modes with $k\eta > 0.2$, i.e.,$l_c < 15.7\eta$, could be regenerated from low wave-number modes. In other words, the target vortex scale should be larger than this critical scale, 15.7η, otherwise the effect of initial errors or uncertainties on the vortex formation cannot be negligible. This condition is used as an indicator that shows the limit of the inertial subrange. The target scales, $l_c = 111.6\eta$, 55.8η, and 27.9η, satisfy this condition and, thus, these scales are considered to be within the inertial subrange. On the other hand, the scale 13.9η does not satisfy the condition, which suggests contamination from the energy-dissipation range exists in this scale.

B. Identification of vortical structures of various scales

A Fourier bandpass filter with a sharp cutoff function is employed for the extraction of the vorticity field of a certain scale from the entire turbulent field [22,23]. The filtered vorticity field

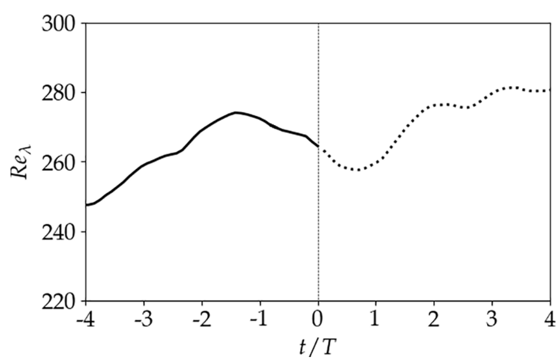

FIG. 1. Time evolution of turbulent Reynolds number based on Taylor microscale, Re_λ. Dotted line for $t/T > 0$ indicates the case in which vortex suppression is not applied.

TABLE II. Time-averaged statistical properties of turbulent field. E is the total energy, Re_λ the Taylor-microscale Reynolds number, ϵ the energy-dissipation rate, l_0 the integral scale, T the large-eddy turnover time, and η the Kolmogorov length scale.

E	Re_λ	ϵ	l_0	T	η
0.581	267	8.46×10^{-2}	1.23	1.97	4.98×10^{-3}

is expressed as

$$\boldsymbol{\omega}_\mathrm{c}(\boldsymbol{k}) = \begin{cases} \boldsymbol{\omega}(\boldsymbol{k}), & \text{when} \quad k_\mathrm{c}/\sqrt{2} \leqslant |\boldsymbol{k}| < \sqrt{2}k_\mathrm{c} \\ 0, & \text{otherwise,} \end{cases} \tag{5}$$

where $\boldsymbol{\omega}_\mathrm{c}$ is the filtered vorticity field in the wave-number space. The filtered vorticity field in the physical space is obtained by an inverse Fourier transformation.

The intense swirling regions in the filtered fields are identified using the Q criterion [35] with a nonzero threshold. The Q criterion has been a widely used vortex identification criterion, such as the Δ [36] and λ_2 [37] criteria. These criteria are capable of capturing mostly similar structures in an isotropic turbulence as far as the intense vortices are targeted [38]. The threshold, Q_th, is set as $Q_\mathrm{th} = 0.75\Omega$, where Ω denotes the rms of the enstrophy density of the filtered vorticity field. The value is empirically chosen based on the observation of the identified vortical structures to exclude inactive vortices that may be insignificant for the dynamics of vortices, although some arbitrariness remains in the selection of the value. A sensitivity analysis for the threshold value was performed by Hirota *et al.* [23] within a range of $0.5\Omega \leqslant Q_\mathrm{th} \leqslant 1.0\Omega$, which showed that the choice of the threshold was insensitive to the analytical results and did not change the conclusions of the study.

The vortical structures at $t/T = 0$ in the original field and the filtered fields, whose central wave numbers are $k_\mathrm{c} = 4\sqrt{2}$, $8\sqrt{2}$, $16\sqrt{2}$, and $32\sqrt{2}$, which correspond to the length scales of $l_\mathrm{c} = \pi/k_\mathrm{c} = 111.6\eta, 55.8\eta, 27.9\eta$, and 13.9η, respectively, are shown in Fig. 3. For quantitative analysis of the dynamics of the vortical structures, each vortex is reconstructed into a group of regularized parts of the vortex, referred to as the vortex segments, which are arranged along the vortical axis [23]. Here, the line connecting the local maximum points of Q ($\geqslant Q_\mathrm{th}$) is regarded as the central axis of a vortex. The detailed procedure is briefly summarized below.

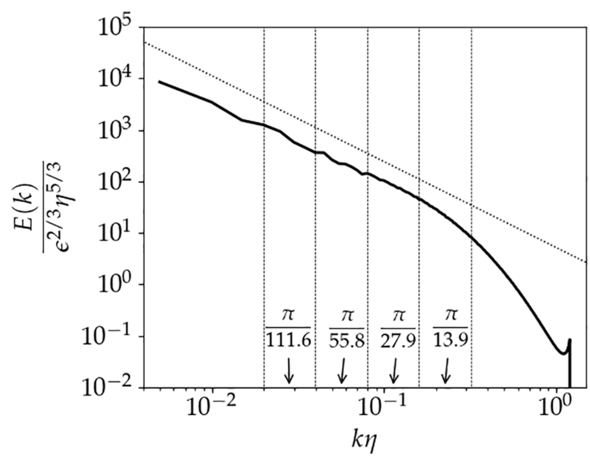

FIG. 2. Energy spectrum of a turbulent field at $t/T = 0$. Arrows and vertical broken lines indicate center wave number and wave-number band of Fourier bandpass filters, which correspond to length scales 111.6η, 55.8η, 27.9η, and 13.9η. Dotted line denotes $k^{-5/3}$ slope.

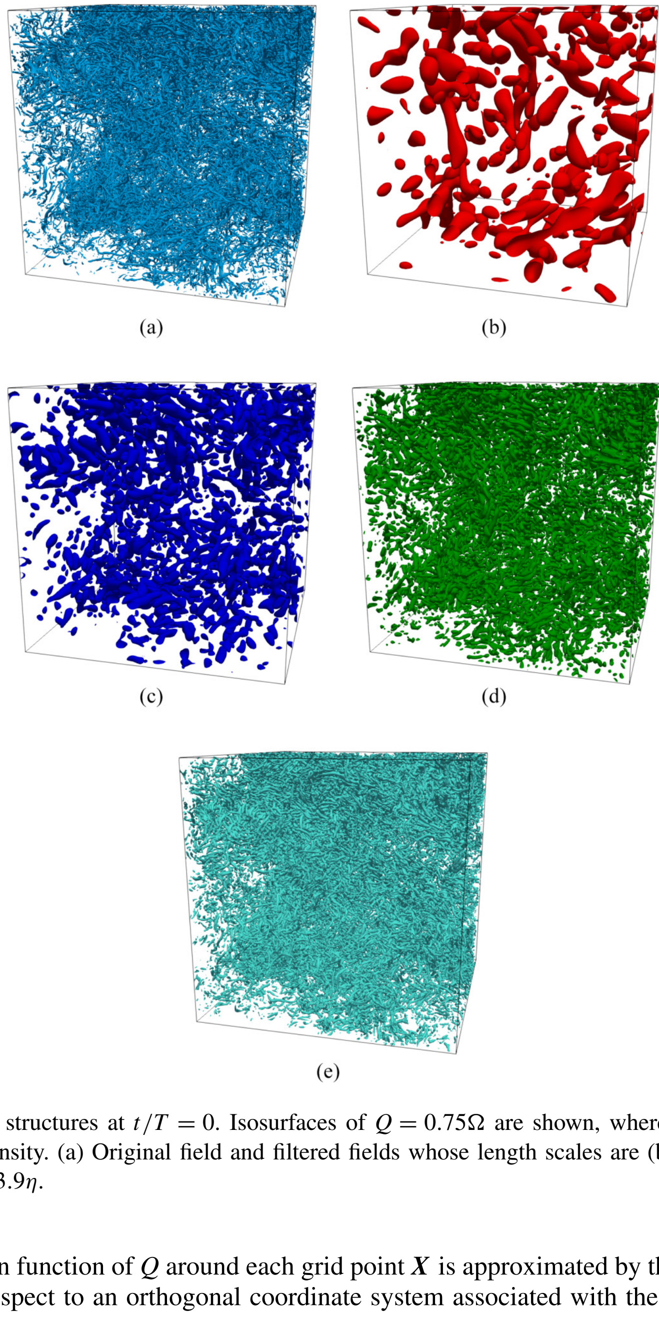

FIG. 3. Vortical structures at $t/T = 0$. Isosurfaces of $Q = 0.75\Omega$ are shown, where Ω denotes the rms of the enstrophy density. (a) Original field and filtered fields whose length scales are (b) 111.6η, (c) 55.8η, (d) 27.9η, and (e) 13.9η.

The distribution function of Q around each grid point $\boldsymbol{X}$ is approximated by the quadratic Taylor expansion with respect to an orthogonal coordinate system associated with the eigenvector of the Hessian of Q,

$$Q(\boldsymbol{x}_e) = Q(\boldsymbol{X}_e) + \nabla_e Q \cdot \boldsymbol{h} + \tfrac{1}{2} H_e(Q)\boldsymbol{h}^t \boldsymbol{\Lambda}\boldsymbol{h}, \tag{6}$$

where $\boldsymbol{\Lambda} = (\lambda_1, \lambda_2, \lambda_3)$ are the eigenvalues of the Hessian of Q, and $\boldsymbol{h} = \boldsymbol{x}_e - \boldsymbol{X}_e$ and the subscript e denotes the values of the transformed coordinate system. The vector $\boldsymbol{h}$ is regarded as a column vector when matrices are involved. When the eigenvalues are sorted in the order of $\lambda_1 \geqslant \lambda_2 \geqslant \lambda_3$, the value of λ_2 becomes negative at a point on the vortex axis, which indicates that Q has a local maximum in the plane normal to the e_1 axis. Let $\boldsymbol{c}$ be the local maximum point, $c_1 = X_{e1}$ and (c_2, c_3)

is obtained by solving the equation so $(\partial Q/\partial e_2, \partial Q/\partial e_3) = (0, 0)$ as

$$\nabla_e Q(\boldsymbol{x}_e)^t = \nabla_e Q(\boldsymbol{X}_e)^t + \boldsymbol{\Lambda h}^t = 0. \tag{7}$$

Each vortex axis is then constructed by connecting these neighboring candidates under two restraining conditions; the distance between the two points should be less than three grid widths, and the angle between two connecting lines must be less than 45°. A minute vortex axis shorter than the averaged diameter of the axis components is regarded as noise and discarded.

A vortex is represented as $\Pi_s = \{s_i | (1 \leqslant i \leqslant n_s)\}$, where s_i denotes a vortex segment and n_s is the number of the vortex segments that compose the vortex. The diameter, D, and length, l, of the vortex are defined as

$$D = \frac{1}{n_s}\sum_{i=1}^{n_s} D_{s_i}, \tag{8}$$

$$l = \sum_{i=1}^{n_s-1} |\boldsymbol{x}_{s_{i+1}} - \boldsymbol{x}_{s_i}|, \tag{9}$$

where D_{s_i} and $\boldsymbol{x}_{s_i}$ are the diameter and position vector of the vortex segment s_i.

Assuming that the vorticity distribution is given by the Gaussian profile, the value of D_{s_i} can be estimated as the azimuthal average of the scale parameters $a(0 < a \leqslant \pi/4)$ of the Mexican-hat wavelet in the plane normal to the axis of the vortex segment:

$$\frac{D}{2} = \frac{1}{2\pi}\int_0^{2\pi} (\max_a Z(a, \theta)) d\theta. \tag{10}$$

The function $Z(a, \theta)$ is the correlation distribution function in a polar coordinate system given by

$$Z(a, \theta) = \frac{\langle \psi(a), \omega_{pe}(\theta)\rangle}{a} = \frac{1}{a}\int_0^{\infty} \psi(r, a)\omega_{pe}(r, \theta) dr, \tag{11}$$

where $\psi(r, a)$ is the mother wavelet and ω_{pe} is the vorticity normalized using its absolute value at the origin.

The average curvature ρ of vortex Π_s is calculated from the radii of circles which are defined by three adjacent segments as

$$\rho = \frac{1}{n_s - 2}\sum_{i=1}^{n_s-2} \frac{4A_{s_i}}{d_1 d_2 d_3}, \tag{12}$$

$$A_{s_i} = \sqrt{a(a - d_1)(a - d_2)(a - d_3)}, \tag{13}$$

$$a = \frac{d_1 + d_2 + d_3}{2}, \tag{14}$$

$$d_1 = |\boldsymbol{x}_{s_{i+1}} - \boldsymbol{x}_{s_i}|, \quad d_2 = |\boldsymbol{x}_{s_{i+2}} - \boldsymbol{x}_{s_{i+1}}|, \quad d_3 = |\boldsymbol{x}_{s_i} - \boldsymbol{x}_{s_{i+2}}|. \tag{15}$$

The numbers of vortices reconstructed from the filtered flow fields shown in Fig. 3 are 313, 1 966, 11 276, and 43 550 for the cases $l_c = 111.6\eta$, 55.8η, 27.9η, and 13.9η, respectively.

The temporal evolution of the vortical structures in the filtered fields when the energy-damping force, $\boldsymbol{f}_2$, is not applied is used as the reference data set. A consecutive data set of the turbulent field in $(-4 \leqslant t/T \leqslant 4)$ with the time interval of $\tau/10$ is used for the analysis, where τ is the Kolmogorov time. The normalized occurrences of the diameters of the vortices, D, are plotted in Fig. 4(a). The diameters are normalized by the corresponding length scales of the center wave numbers of the filters, l_c. The normalized diameters are found to be distributed mostly around $D/l_c = 1$, regardless of the filtering scale. Figure 4(b) shows the normalized occurrences of aspect ratios $\alpha = l/D$ of the vortices weighted by their volumes. When evaluating the existence probability of vortices with specific aspect ratios at a certain scale, it would be preferable to consider each vortex

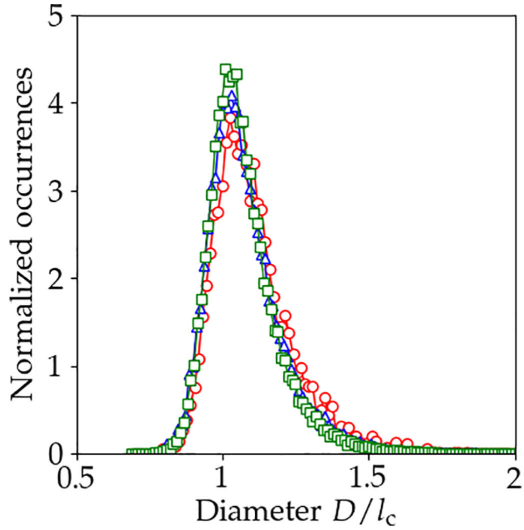

(a)

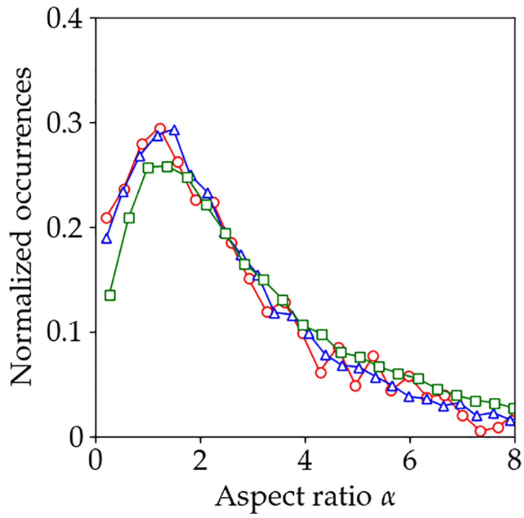

(b)

FIG. 4. (a) Normalized occurrences of diameters of vortices, D, obtained from filtered fields. (b) Normalized occurrences of aspect ratios, α, of vortices weighted by their volumes. Length scales of filtered fields are 111.6η; —○—, 55.8η; —△—, 27.9η; —□—.

volume in addition to the number of vortices because larger vortices occupy a greater proportion of the domain and their induced velocity fields spread over a wide area. Although the peaks appear around $\alpha = 1.5$, the aspect ratios are broadly distributed regardless of the filtering scales. The peaks of the frequency distributions may depend on the choice of the filter and the threshold of the vortex identification method; however, it is shown that the frequency distribution of the aspect ratios is independent of the scales of vortices as long as the bandwidths of the filter and the thresholds for the vortex identification are equivalently chosen. These statistical results indicate that the shapes of the vortices are quite similar, regardless of their scales, or, in other words, the hierarchical vortical structures in the inertial subrange are self-similar.

C. Definition of energy-damping force

The coherent structures that transfer kinetic energy from larger to smaller scales are observed intermittently in turbulent flows. The Fourier bandpass filter is useful to extract these structures of a certain scale; however, simply suppressing such Fourier components is inadequate for discussing the role of vortex motion on the energy cascade process, because the phase information required for their reconstruction is lost in Fourier space. Thus, after the target vortices are extracted from the filtered field using the Q criterion, we chose to suppress the rotational motions in the extracted structures by the energy-damping force. The energy-damping force, $\boldsymbol{f}_2$, is given as

$$\boldsymbol{f}_2 = -cW_{\mathrm{kc}}(\boldsymbol{x}, t)\boldsymbol{u}_{\mathrm{kc}}(\boldsymbol{x}, t), \tag{16}$$

where c is a nondimensional parameter related to the magnitude of the external force, and $\boldsymbol{u}_{\mathrm{kc}}(\boldsymbol{x}, t)$ is the velocity field extracted using Eq. (5) with the center wave number of k_{c}. The minus sign on the right-hand side signifies that the force is given in the opposite direction to the velocity vector. $W_{\mathrm{kc}}(\boldsymbol{x}, t)$ is the distribution function of the force that is defined as

$$W_{\mathrm{kc}}(\boldsymbol{x}, t) = \begin{cases} \sqrt{Q_{\mathrm{kc}}(\boldsymbol{x}, t)}, & \text{where} \quad Q_{\mathrm{kc}}(\boldsymbol{x}, t) > 0 \\ 0, & \text{otherwise}, \end{cases} \tag{17}$$

where $Q_{\mathrm{kc}}(\boldsymbol{x}, t)$ is the Q value for the filtered velocity field, $\boldsymbol{u}_{\mathrm{kc}}(\boldsymbol{x}, t)$, of k_{c} scale. In Eq. (16), $W_{\mathrm{kc}}(\boldsymbol{x}, t)$ confines the target of the force within the vortices in the physical space, and $\boldsymbol{u}_{\mathrm{kc}}(\boldsymbol{x}, t)$ confines the target of the force within a certain scale band in the wave-number space. The energy-damping force, $\boldsymbol{f}_2$, has the dimension of acceleration. In summary, the force $\boldsymbol{f}_2$ decelerates the fluid motions only inside the vortices of a certain scale.

The target length scale, l_{t}, of the energy-damping force is set as $l_{\mathrm{t}} = 27.9\eta$ ($k_{\mathrm{t}} = 16\sqrt{2}$), and vortex motions on this scale are forcibly suppressed using Eq. (16). Then, the response of the energy spectrum and the vortical motions, whose scales are either smaller or larger than the target scale, namely $l_{\mathrm{c}} = l_{\mathrm{t}}/2$ $(= 13.9\eta)$, $2l_{\mathrm{t}}$ $(= 55.8\eta)$, and $4l_{\mathrm{t}}$ $(= 111.6\eta)$ are studied. The energy-damping force, $\boldsymbol{f}_2$, is activated at $t/T = 0$ and continuously applied afterward, whereas the driving force of the turbulent field, $\boldsymbol{f}_1$, is continuously applied throughout the simulation. On the basis of the preliminary computations, the magnitude of the damping force, c in Eq. (16), is determined so the net energy-damping rate at $t/T = 0$, $\boldsymbol{f}_2(0) \cdot \boldsymbol{u}^*(0)$, becomes $\boldsymbol{f}_2(0) \cdot \boldsymbol{u}^*(0) = 10\epsilon$. Here, $*$ denotes the complex conjugate. When $\boldsymbol{f}_2$ is too weak, e.g., 1ϵ, many structures still remain and the target vortex motions cannot be adequately suppressed, while too strong a damping rate, such as 50ϵ, definitely weaken the target vortices; however, such excessive force supplies additional energy into the vortices half the target scale and compensates the energy loss in this range. The response of the energy spectrum is discussed later in Fig. 10.

D. Vortex tracking method

In inviscid flow cases, vortices can be tracked in a deterministic way using the Helmholtz vorticity theorem because vortex lines are fixed to fluid particles, and their topology is conserved. However, such a unique solution that describes the evolution of vortex tubes and surfaces does not exist for viscous flows. Thus, a proper tracking method is necessary to discuss the dynamics of vortical structures that comprise a turbulent field.

Vortex tracking is a complex issue, as the size and length of individual vortices are widely distributed even for filtered fields (Fig. 4). In addition, their shapes change with time, and their motions include various events, such as generation, stretching, splitting, merging, and breakdown. Except for Pullin and Yang [39], where a set of equations describing the evolution of vortex surface fields starting from a known initial condition with a method analogous to a predictor-corrector approach was used, most methods are based on rather practical approaches, which are similar to techniques used in image processing [28–31].

In this paper, the individual vortices in the filtered fields are tracked in a Lagrangian framework. First, an attempt is made to reconstruct the vortices into vortex segments. However, using this

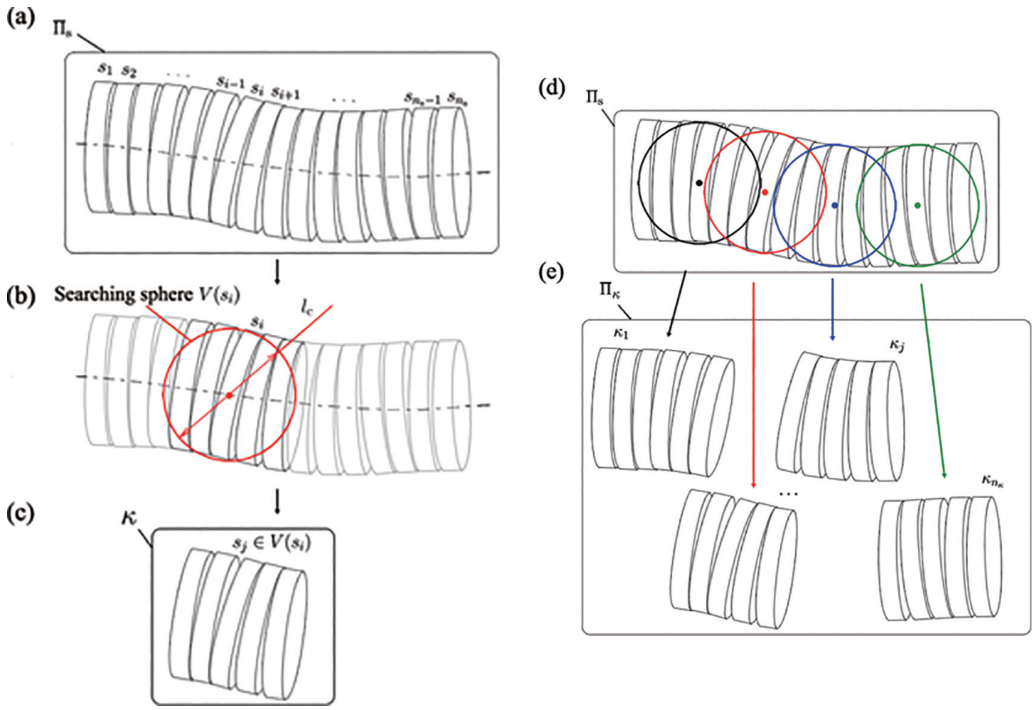

FIG. 5. Sketch of procedure to subdivide a vortex. (a) A vortex is replaced by a group of vortex segments $s_i \in \Pi_s$. (b) A searching sphere $V(s_i)$ with characteristic diameter, l_c, and its center at position of s_i is defined. (c) Vortex segments $s_j \in V(s_i)$ are grouped into a vortex unit, κ. (d) When all vortex segments s_i are grouped into vortex units, (e) coarse-graining of a vortex into a group of vortex units, κ_j, is complete.

method, catching a segment in a certain time step and finding the corresponding segment in the next time step become difficult. This is mainly a result of the lengths of the segments being too short as well as their volumes being too small. Thus, this method requires a short time step. Additionally, tracking a large number of vortex segments consumes a large amount of computational power. To overcome this problem, a vortex unit, which is also a section of a divided vortex, although much larger than the vortex segment, is introduced. Each vortex is represented by a group of vortex units. The aspect ratio of a vortex unit is roughly one. A vortex unit includes several vortex segments and, thus, the number of vortex units in the flow field is much smaller than that of the vortex segments. This treatment significantly reduces the computational cost. And, by tracking the vortex units, there is no need to be concerned with events such as splitting and merging, which drastically change the shape of a vortex. The tracking process consists of two stages: coarse-graining (stage 1) and temporal tracking (stage 2). The details of each step are described below.

1. Stage 1. Coarse graining

In this stage, the vortices are subdivided into groups of vortex units. Figure 5 shows a sketch which demonstrates the procedure to subdivide a vortex.

(I) A set of vortex segments, which composes a target vortex, is shown in Fig. 5(a),

$$\Pi_s = \{s_i | 1 \leqslant i \leqslant n_s \ (n_s \text{ is a non-negative integer})\}, \tag{18}$$

where s_i is a single vortex segment.

(II) A spherical region $V(s_i)$ of diameter l_c with its center at the center of vortex segment $s_i \in \Pi_s$ is defined, as shown in Fig. 5(b). Here, the diameter l_c is the corresponding length scale of the filtered field.

(III) A set of vortex segments inside the spherical region $s_j \in V(s_i)$ is defined as the vortex unit κ, as shown in Fig. 5(c). One vortex segment may belong to multiple vortex units.

(IV) Another vortex unit is obtained by applying steps II and III to the remaining vortex segments, which do not belong to any of the vortex units.

(V) Steps II–IV are repeated until all vortex segments are included in one or more vortex units, as shown in Fig. 5(d). In Fig. 5(d), the center of each circle representing a spherical region $V(s_i)$ is also the center of the vortex segment s_i, which is chosen as the central segment. As a result, as shown in Fig. 5(e), a vortex Π_s is coarse-grained into a set of vortex units κ_j as

$$\Pi_\kappa = \{\kappa_j | 1 \leqslant j \leqslant n_\kappa \ (n_\kappa \text{ is a non-negative integer})\}. \tag{19}$$

Here, vortex units whose aspect ratio is less than 0.5 are discarded as noise. The diameter and length of each vortex unit are calculated using Eqs. (8) and (9) against all vortex segments within the vortex unit.

(VI) The position $\boldsymbol{x}_{\kappa_j}(t)$ and convection velocity $\boldsymbol{v}_{\kappa_j}(t)$ of vortex unit $\kappa_j(t)$ at time t are defined using the average of the vortex segments that are members of κ_j,

$$\boldsymbol{x}_{\kappa_j}(t) = \sum_{k=1}^{m_{\kappa_j}} \boldsymbol{x}_{s_k}(t)/m_{\kappa_j}, \tag{20}$$

$$\boldsymbol{v}_{\kappa_j}(t) = \sum_{k=1}^{m_{\kappa_j}} \boldsymbol{v}_{s_k}(t)/m_{\kappa_j}, \tag{21}$$

where $\boldsymbol{x}_{s_k}$ and $\boldsymbol{v}_{s_k}$ are the position vector and velocity vector of a vortex segment s_k ($k = 1, \cdots, m_{\kappa_j}$) in $\kappa_j(t)$, respectively.

2. Stage 2. Temporal tracking

A tracking of the coarse-grained vortices is performed using the following numbered procedures. Figure 6 demonstrates a sketch of the vortex tracking method.

(I) The position of the vortex unit $\kappa_j(t+\delta t)$ after a short time interval δt is predicted using the convection velocity as

$$\boldsymbol{x}_{\kappa_j}(t+\delta t) = \boldsymbol{x}_{\kappa_j}(t) + \boldsymbol{v}_{\kappa_j}(t)\delta t. \tag{22}$$

(II) A spherical searching area of diameter l_c is created with its center at the predicted position $\boldsymbol{x}_{\kappa_j}(t+\delta t)$. Then the vortex segments Π_s of time $t+\delta t$ inside the searching sphere are regarded as vortex segments forming the vortex unit $\kappa_j(t+\delta t)$ at $t+\delta t$. If no vortex segment is found inside the spherical searching area, the lifespan of the vortex unit is regarded as being over. Steps I and II are repeated advancing the time until all vortex units become untraceable. The same procedure is also carried out, advancing time in the opposite direction, until no corresponding vortex unit could be found.

Through the two stages given above, each part of the vortices observed at time t can be tracked from the cradle to the grave. The lifespans of vortex units, T_l, are defined as the time differences between the beginnings of the vortex tracking and their ends. Notably, the choice of the diameter of the searching sphere, l_c, is somewhat arbitrary. Here the diameter, l_c, is set to the length corresponding to the center wave numbers of the filter used to extract the flow field.

Figure 7 is an example of temporal tracking of vortices for three different scales: $l_c = 111.6\eta$, 55.8η, and 27.9η, colored by red, blue, and yellow, respectively. Although the flow field is packed with many vortex units at $t/T = 0$ (c), their numbers gradually decreases as time progresses or by going back in time, especially for smaller-scale units.

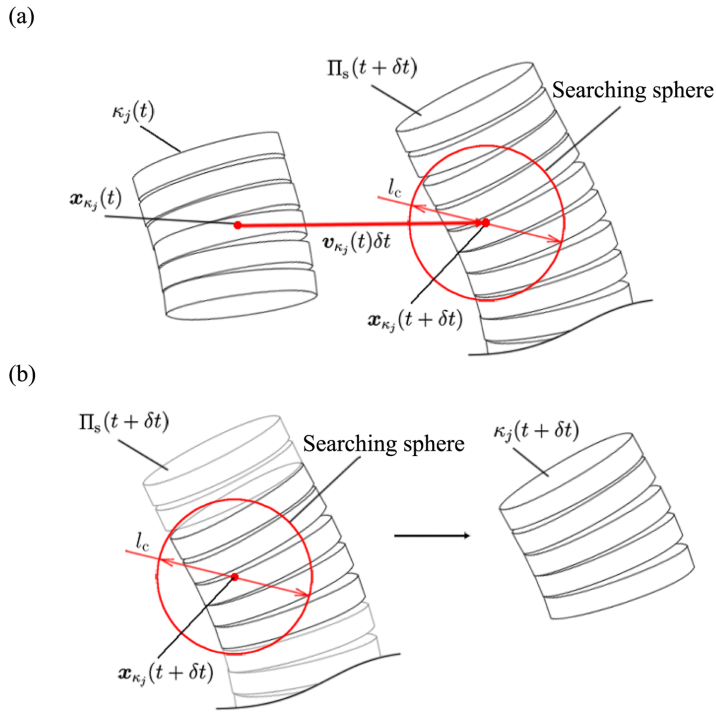

FIG. 6. Sketch of vortex tracking method. (a) Position $\boldsymbol{x}_{\kappa_j}(t)$ and velocity $\boldsymbol{v}_{\kappa_j}(t)$ of vortex unit κ_j is evaluated, and its position at $t+\delta t$ is estimated as $\boldsymbol{x}_{\kappa_j}(t+\delta t) = \boldsymbol{x}_{\kappa_j}(t) + \boldsymbol{v}_{\kappa_j}(t)\delta t$. Then, a searching sphere with characteristic diameter, l_c, is defined at $\boldsymbol{x}_{\kappa_j}(t+\delta t)$. $\Pi_s(t+\delta t)$ is a group of vortex segments found at $t+\delta t$ whose members are within the searching sphere. (b) Vortex segments inside the searching sphere are grouped and regarded as the vortex unit κ_j at the next time $t+\delta t$.

E. Verification of proposed tracking method

Figure 8 shows the normalized occurrences of the diameters, D, and the aspect ratios, α, of vortex units weighted by their volumes. The diameter distributions are identical to those of the vortex segments shown in Fig. 4(a), agreeing with the fact that vortex units consist of vortex segments. The aspect ratios of the vortex units are in the range of 0.5–1.5, as intended. The major peaks of the aspect ratios are found at approximately $\alpha = 1.2$, irrespective of the filtering scales. It should be noted that the lower peaks around $\alpha = 0.6$ correspond to the vortex units found near the ends of vortices. The vortex units near the ends of the vortices tend to be shorter and contain a smaller number of segments. From these results, it is confirmed that the vortical structures filtered at each scale are appropriately reconstructed by groups of vortex units.

The lifespans of vortex units, T_l, in the target turbulent field are estimated to validate the present tracking method. The results are shown in Fig. 9 for three filtered fields. The timestep for vortex tracking is set to $\tau/10$, where τ is the Kolmogorov time. The obtained lifespan is normalized by the eddy turnover time of each filtered field, $T_c = l_c^{2/3}\epsilon^{-1/3}$. The profiles show large peaks around $T_l/T_c = 0.4$–0.8. The peak lifespan for the largest scale $l_c = 111.6\eta$ is slightly longer, which is likely due to contamination from the energy-containing range. The values obtained are consistent with the lifespan of coherent structures of isotropic turbulence reported by Cardesa *et al.* [28]. Therefore, we evaluated that our present method appropriately tracks the motions of the vortices. The advantage of the proposed method is that it can analyze the lifespan of each vortex, as each vortex is individually tracked.

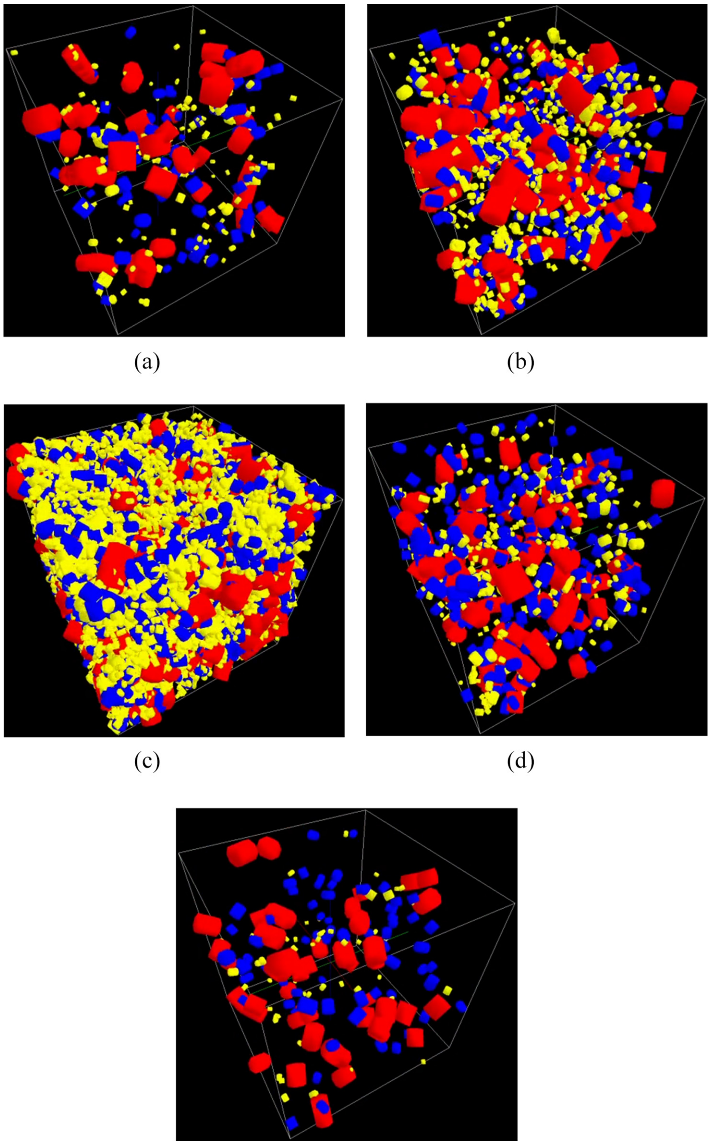

FIG. 7. Snapshots of tracked vortex units at $t/T = -1$ (a), -0.5 (b), 0 (c), 0.5 (d), and 1 (e). Each vortex unit at $t/T = 0$ is tracked from the cradle to the grave. Red, blue, and yellow units represent three different length scales, 111.6η, 55.8η, and 27.9η, respectively.

III. RESPONSE OF TURBULENT FIELD TO APPLICATION OF ENERGY-DAMPING FORCE

Figure 10 shows the temporal response of the energy spectrum when the energy-damping force, $\boldsymbol{f}_2$, is applied. The damping force is intended to suppress the vortical motions of the target scale of $l_{\mathrm{t}} = 27.9\eta$. The timescale is normalized by the large-eddy turnover time, T. The energy slightly increases in the neighboring low wave-number (large scale) range, while it decreases in the high wave number (small scale) range. The ratio of the total kinetic energy at $t/T = 0$ to that at $t/T = 4$

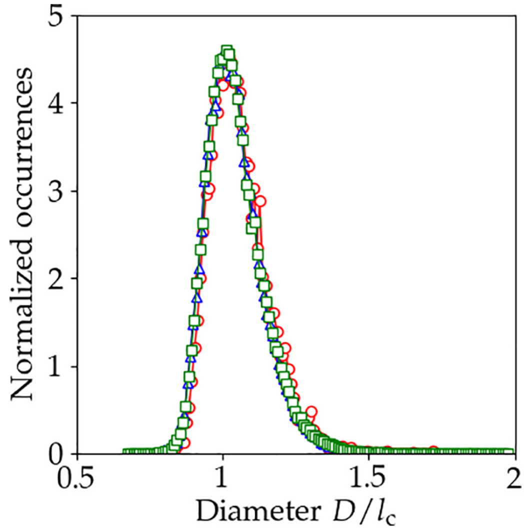

(a)

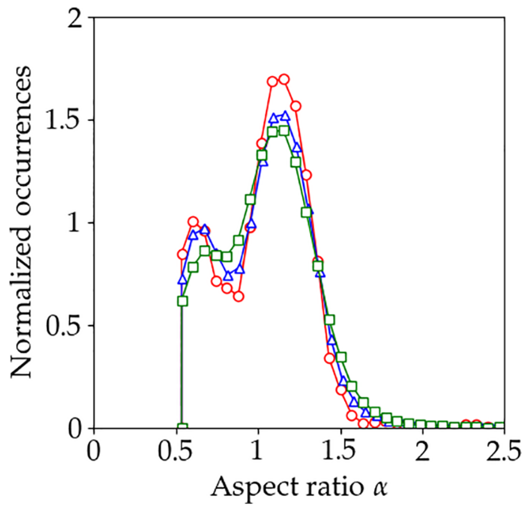

(b)

FIG. 8. (a) Normalized occurrences of diameters of vortex units, D, obtained from filtered fields. (b) Normalized occurrences of aspect ratios, α, of vortex units. Length scales of filtered fields are 111.6η; —○—, 55.8η; —△—, 27.9η; —□—.

is 1.03. This response is expected, as the energy transfer from the large scale to the small scale is cut off by the suppression of the vortical motions of the target scale.

Next, the relationship between the change in the energy spectrum and the vortex motions is analyzed. Figure 11 shows the vortical structures at $t/T = 4$ for the original field and four different scales: the target scale, l_t; twice the scale, $2l_t$; four times the scale, $4l_t$; and half the scale, $l_t/2$. The target-scale vortices almost entirely disappear, which corresponds to the decrease in energy shown in Fig. 10. In the large-scale range, the vortical structures become slightly denser than those at $t/T = 0$ (Fig. 3), while they become sparse in the small-scale range. The changes to the vortical

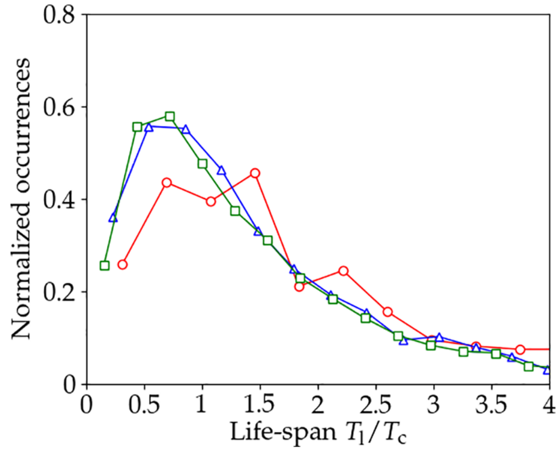

FIG. 9. Normalized occurrences of normalized lifespan of vortex units, T_l. Length scales of filtered fields are: 111.6η; , 55.8η; , 27.9η; .

structures of various scales are consistent with the corresponding responses found in the energy spectrum.

Figure 12 shows the normalized occurrences of the stretching speeds of the vortex segments whose scales are half the target scale. The stretching speeds before and after the suppression of the target vortex motions are compared. The stretching speeds, γ, are calculated using the following equation:

$$\gamma = \frac{1}{n_s - 1} \sum_{i}^{n_s-1} \frac{|(\boldsymbol{x}_{s_i} + \boldsymbol{u}(\boldsymbol{x}_{s_i})\delta t) - (\boldsymbol{x}_{s_{i-1}} + \boldsymbol{u}(\boldsymbol{x}_{s_{i-1}})\delta t)| - |\boldsymbol{x}_{s_i} - \boldsymbol{x}_{s_{i-1}}|}{|\boldsymbol{x}_{s_i} - \boldsymbol{x}_{s_{i-1}}|\delta t}, \tag{23}$$

where $\boldsymbol{u}(\boldsymbol{x})$ is the velocity field of the whole turbulent field. The stretching speeds are normalized by the eddy turnover time, T_c. In the figure, the peak positions of the distributions do not change before

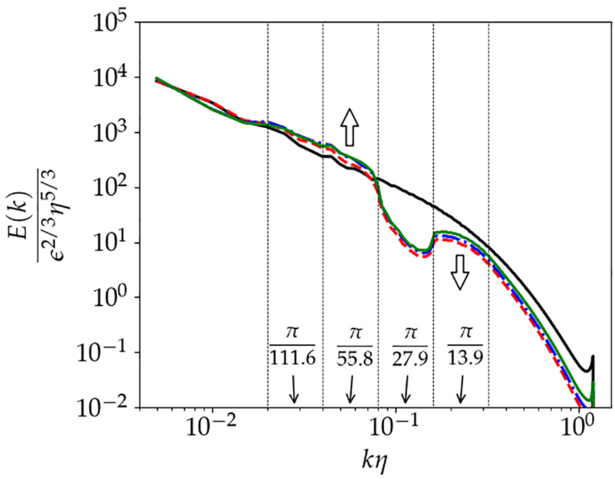

FIG. 10. Temporal response of energy spectrum at $t/T = 0$, ; 1, ; 3, ; 4, . Vertical broken lines denote the wave-number band of Fourier bandpass filter whose corresponding length scales are 111.6η, 55.8η, 27.9η, and 13.9η.

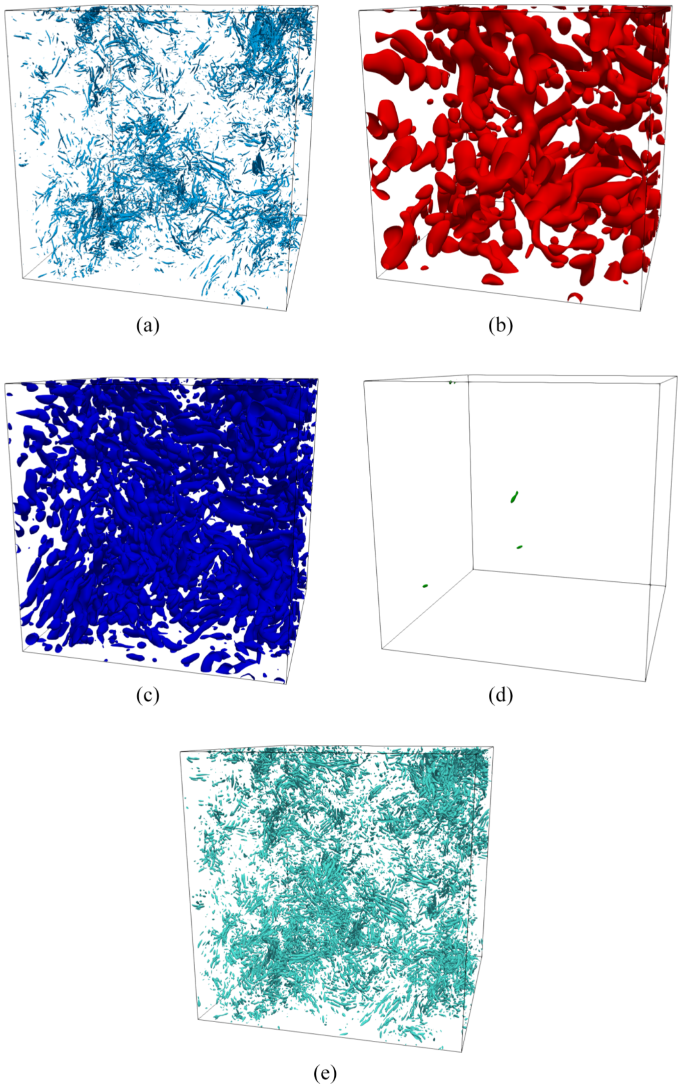

FIG. 11. Vortical structures in at $t/T = 4$ when vortical motions of length scale 27.9η are suppressed. Isosurfaces of $Q = 0.75\Omega$ are shown. Values of threshold are same as in Fig. 3. (a) Original field and filtered fields whose length scales are (b) 111.6η, (c) 55.8η, (d) 27.9η, and (e) 13.9η.

and after the suppression. However, the positive side values tend to decrease more than the negative side values after the suppression, lowering the averaged stretching speed from 0.552 at $t/T = 0$ to 0.462 at $t/T = 4$. Therefore, the averaged stretching speed declines approximately 20% as a result of the suppression. In other words, the vortices half the target scale, $l_t/2 = 13.9\eta$, were strongly stretched by the vortices of the target scale, $l_t = 27.9\eta$, when the damping force was absent. This result supports the fact that the vortices of a certain scale tend to be stretched by vortices twice their size [18,20,22,23]. In conclusion, the decrease in the kinetic energy in the small scale regions can be attributed to the decrease in the stretching speeds of the vortices.

The time variations of the number of vortices of each scale are shown in Fig. 13. The data for the cases without the energy-damping force are also presented as dotted lines in the figure for comparison. The number of vortices of the target scale, $l_t = 27.9\eta$, whose motions are forcibly

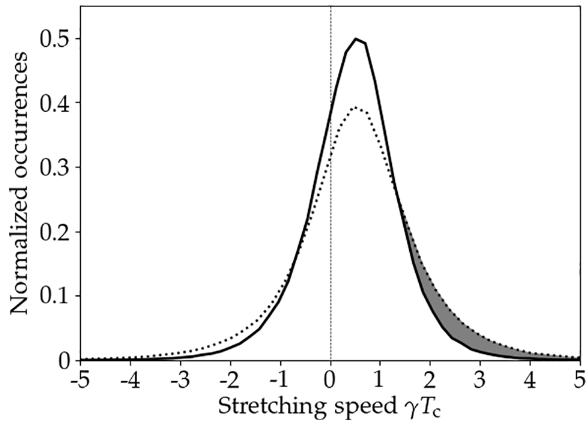

FIG. 12. Normalized occurrences of stretching speeds of vortex segments, γ, on scale 13.9η at $t/T = 0$ (dotted line) and $t/T = 4$ (solid line) when vortical motions of length scale 27.9η are suppressed.

suppressed, sharply decreases accompanying the suppression. Once the flow field is adapted to the changed environment with 27.9η scale absent, both the $l_c = 2l_t (= 55.8\eta)$ and $4l_t (= 111.6\eta)$ cases eventually exhibit similar tendencies. The number of vortices that are twice as large as the target scale, $l_c = 2l_t (= 55.8\eta)$, first decreases until around $t/T = 0.5$, and then increases until reaching a constant value of approximately 2 700 around $t/T = 2$. The temporal decrease at the beginning may have been caused by the leakage of the energy-damping force applied to the target scale. Because the cutoff function of the Fourier bandpass filters is sharp, the Fourier components representing the vortical structures whose scales are twice as large as the target scale might be contaminated by the energy-damping force at the target scale. This is a limitation of the procedure used in this numerical experiment. For vortices that are four times as large as the target scale, $l_c = 4l_t (= 111.6\eta)$, the number monotonically increases and reaches a constant value of approximately 500 around $t/T = 2$. In this case, the leakage does not occur, which is likely a result of the scales being apart. For both length scales, the timescales of the changes are in the order of the large-eddy turnover time, T, which is much longer than the turnover time of vortices in each scale. Figures 13 and 14 indicate that since the energy cascade system is intrinsically driven by large eddies in the energy-containing

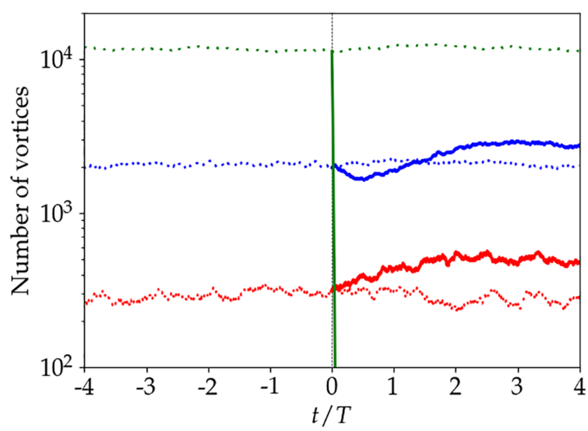

FIG. 13. Time variations of number of vortices when vortical motions on scale 27.9η are suppressed by energy-damping force (solid line). Colors reflect length scales of vortices: red, 111.6η; blue, 55.8η; green, 27.9η. Dotted lines indicate the cases in which energy-damping force is not applied.

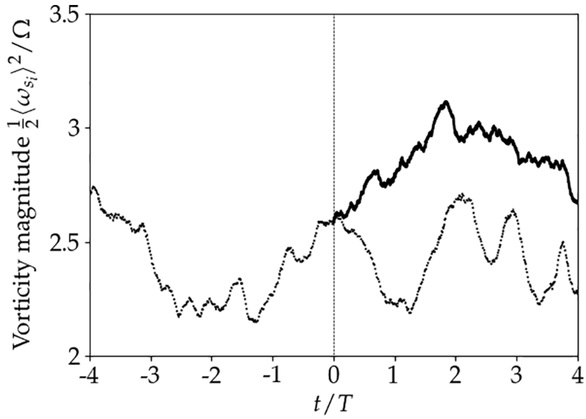

(a)

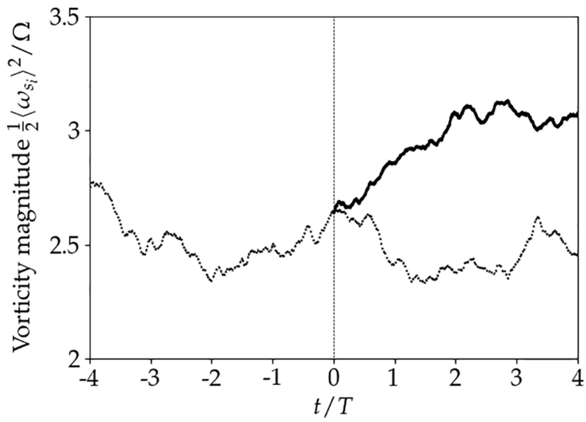

(b)

FIG. 14. Time variations of averages of vorticity magnitudes at centers of vortex segments when vortical motions of scale 27.9η are suppressed by energy-damping force (solid line). Length scales of vortex segments are (a) 111.6η and (b) 55.8η. Dotted lines indicate the case in which energy-damping force is not applied.

range, the timescale required for adjusting the system to a given environment is inevitably on the order of the large-eddy turnover time.

The time variations of the averages of vorticity magnitudes at the centers of the vortex segments, $\langle\omega_{s_i}\rangle$, are plotted in Fig. 14. The scales of vortices are (a) four times and (b) twice as large as that of the scale of vortices in which the energy-damping force is applied, $l_t = 27.9\eta$. The values are normalized using the rms of the enstrophy density of each filtered field, Ω, at $t/T = 0$. In both cases, when the energy-damping forces are applied, the vorticity magnitudes increase for two large-eddy turnover times (shown in solid lines). For the case of vortices twice the scale, the value appears to reach a constant, which is approximately 20% greater than before the application of the energy-damping force. These results indicate that the increase in the energy in the low wave-number ranges, as ishown in Fig. 10, is due to the increase in the number and magnitude of the vortices. Judging from the energy spectrum, the scale of 13.9η is too close to the energy dissipation range to quantitatively discuss the vortical structures in this scale. Thus, this scale is excluded from the discussion. To discuss the structures whose scales are smaller than the damped scale, higher Reynolds-number database is required. This remains a future task.

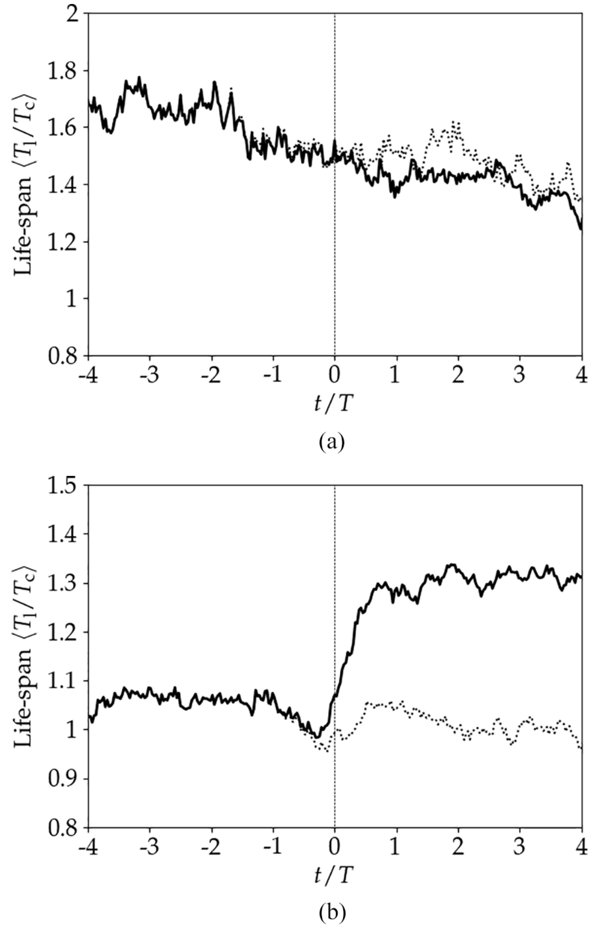

FIG. 15. Time variations of normalized lifespans of vortex units when vortical motions on scale 27.9η are suppressed by energy-damping force (solid line). Length scales of vortices are (a) 111.6η and (b) 55.8η. Dotted lines indicate the case in which energy-damping force is not applied.

The time variations of the average lifespan of the vortex units are shown in Fig. 15. Figure 15(b) demonstrates that as for the vortices whose scales are twice as large as the target scale, the lifespans of their vortex units increase by approximately 30%, accompanying the suppression of the target scale vortices. The lifespan of vortices is of the order of the eddy turnover time, T_c, regardless of the scale, which has been confirmed in Fig. 9 and the results reported by Cardesa *et al.* [28]. This trend may be attributed to the balance of the energy flux which is poured into and is drawn from the target scale. By suppressing the target vortices, the interactions which cause the energy transfer are eliminated, allowing the vortices whose scales are twice as large as the target scale to survive longer. Thus, the increase in the lifespans of the vortices that are twice as large as the target scale, i.e.,the delay of their time of death, can be attributed to the absence of target vortex motions.

Moreover, Fig. 16 shows the time variations of the averaged curvature, ρ, of the vortical axes normalized by the corresponding length scales of the filtered fields, which are (a) $l_c = 4l_t$ and (b) $l_c = 2l_t$. In the uncontrolled cases, shown by the dotted lines, the normalized curvatures of the vortical axes are nearly constant at $\langle \rho l_c \rangle =$ 0.5–0.6 for both scales. However, as shown by a solid line in Fig. 16(b), the curvature of the vortical axes sharply decrease when the energy-damping force is applied. This tendency cannot be found in Fig. 16(a), in which the scale of the vortices is

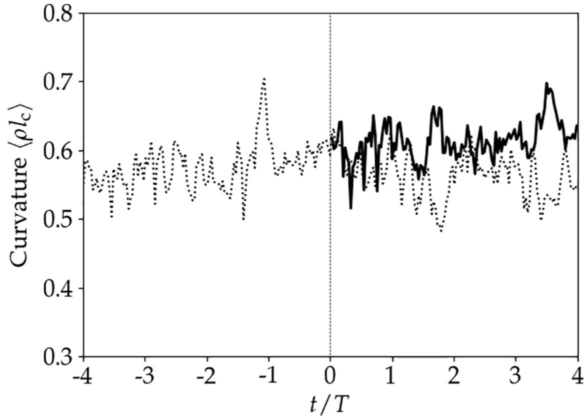

(a)

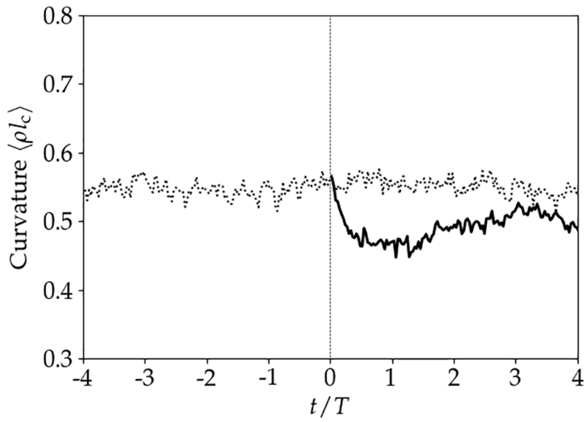

(b)

FIG. 16. Time variations of curvatures of vortical axes when vortical motions on scale 27.9η are suppressed by energy-damping force (solid line). Length scales of vortices are (a) 111.6η and (b) 55.8η. Dotted lines indicate the case in which energy-damping force is not applied.

four times larger than the target scale. This result implies that the vortices of a certain scale in a turbulent field are likely to be deformed by the velocity field induced by vortices of half their scale. The plateau values of the curvature before and after applying the damping force, shown in Fig. 16, may be scaled by the characteristic velocities of vortices whose scales are twice larger or half the target vortices. However, it is left for further analysis in the future.

Figures 15(a) and 16(a) show that the influences among the vortices whose scales are four times different are unclear. The lifespans and shapes of larger vortices appear to be less affected by the suppression of the target scale vortices. The results suggest that the interactions among the vortices mainly occur between those whose scales are very close to one another.

It can be presumed that vortices of a certain scale are constantly deformed by vortices that are half their scale. In addition, their lifespans are likely to be shortened when the deformations take place. The increase in the lifespans of the vortex units, shown in Fig. 15(b), may reflect the weakening of vortex deformation process resulting from the suppression of the half-scaled vortex motions.

The relationship between vortices of a target scale and vortices whose scales are half the target scale are sketched in Fig. 17. The process can be summarized as follows. As is already known, the smaller vortices are likely to be stretched by the neighboring larger vortices in antiparallel

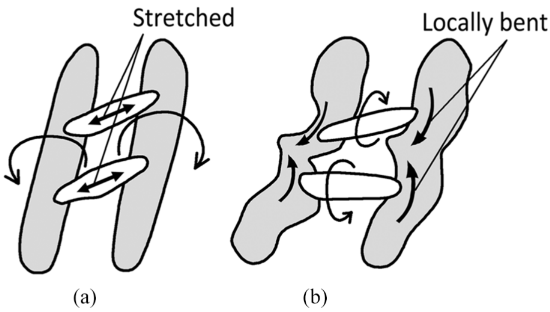

FIG. 17. Sketch of relationship between larger vortices and smaller vortices. (a) Smaller vortices are stretched by larger vortices. (b) Larger vortices are, in return, locally bent by smaller vortices.

arrangement [23], energizing the smaller vortices. At the same time, the larger vortices are locally bent by the smaller vortices shortening their lifespans. Through the process, the turbulent kinetic energy is successively transferred from larger to smaller scales. The dynamics of vortices in turbulent fields has been studied with respect to turbulence-coherent structure interaction [40] and vortex reconnection [41–43]. Investigating the relationship between these findings and the present paper could lead to a deeper understanding of the physical mechanism of the energy cascade in turbulent flows, which will be a subject for future work.

IV. CONCLUSIONS

A numerical experiment was conducted to investigate the role of vortical motion on the energy cascade process in a homogeneous isotropic turbulence. Energy transfer from a large to small scale was suddenly interrupted by artificially suppressing the vortical motions of a certain scale in the inertial subrange. When the target vortices were weakened, the energy increased in the large-scale band and decreased in the small-scale band. The stretching speeds of the vortices whose scales were half of the target scale were reduced as a result of the absence of the target vortices. The response of larger vortical structures was also investigated by tracking individual vortices. It was found that the local curvature of the axes of the vortices twice as large as the target scale vortices decreased, and the life spans of the larger vortices became longer as a result of the suppression of the target scale vortices. These interactions took place only among vortical motions whose scales were close to one another.

ACKNOWLEDGMENT

A part of the results were obtained using supercomputing resources of Cyberscience Center, Tohoku University.

[1] A. N. Kolmogorov, The local structure of turbulence in incompressible viscous fluid for very large Reynolds numbers, Dokl. Akad. Nauk SSSR **30**, 301 (1941).

[2] U. Frisch, P.-L. Sulem, and M. Nelkin, A simple dynamical model of intermittent fully developed turbulence, J. Fluid Mech. **87**, 719 (1978).

[3] T. S. Lundgren, Strained spiral vortex model for turbulent fine structure, Phys. Fluids **25**, 2193 (1982).

[4] A. D. Gilbert, A cascade interpretation of Lundgren's stretched spiral vortex model for turbulent fine structure, Phys. Fluids A: Fluid Dyn. **5**, 2831 (1993).

[5] A. N. Kolmogorov, A refinement of previous hypotheses concerning the local structure of turbulence in a viscous incompressible fluid at high Reynolds number, J. Fluid Mech. **13**, 82 (1962).
[6] J. A. Domaradzki and D. Carati, An analysis of the energy transfer and the locality of nonlinear interactions in turbulence, Phys. Fluids **19**, 085112 (2007).
[7] G. L. Eyink and H. Aluie, Localness of energy cascade in hydrodynamic turbulence. I. Smooth coarse graining, Phys. Fluids **21**, 115107 (2009).
[8] H. Aluie and G. L. Eyink, Localness of energy cascade in hydrodynamic turbulence. II. Sharp spectral filter, Phys. Fluids **21**, 115108 (2009).
[9] R. M. Kerr, Higher-order derivative correlations and the alignment of small-scale structures in isotropic numerical turbulence, J. Fluid Mech. **153**, 31 (1985).
[10] K. Yamamoto and I. Hosokawa, A decaying isotropic turbulence pursued by the spectral method, J. Phys. Soc. Jpn. **57**, 1532 (1988).
[11] Z.-S. She, E. Jackson, and S. A. Orszag, Structure and dynamics of homogeneous turbulence: Models and simulations, Proc. R. Soc. London, Ser. A **434**, 101 (1991).
[12] A. Vincent and M. Meneguzzi, The spatial structure and statistical properties of homogeneous turbulence, J. Fluid Mech. **225**, 1 (1991).
[13] F. Moisy and J. Jiménez, Geometry and clustering of intense structures in isotropic turbulence, J. Fluid Mech. **513**, 111 (2004).
[14] M. Tanahashi, K. Fujibayashi, and T. Miyauchi, Fine scale eddy cluster and energy cascade in homogeneous isotropic turbulence, in *IUTAM Symposium on Computational Physics and New Perspectives in Turbulence*, edited by Y. Kaneda (Springer, Dordrecht, Netherlands, 2008), pp. 67–72.
[15] T. Ishihara, T. Gotoh, and Y. Kaneda, Study of high-Reynolds number isotropic turbulence by direct numerical simulation, Annu. Rev. Fluid Mech. **41**, 165 (2009).
[16] J. Jiménez, A. A. Wray, P. G. Saffman, and R. S. Rogallo, The structure of intense vorticity in isotropic turbulence, J. Fluid Mech. **255**, 65 (1993).
[17] K. Yoshimatsu, K. Anayama, and Y. Kaneda, Influence of vortex dynamics and structure on turbulence statistics at large scales, Phys. Fluids **27**, 055106 (2015).
[18] S. Goto, A physical mechanism of the energy cascade in homogeneous isotropic turbulence, J. Fluid Mech. **605**, 355 (2008).
[19] S. Goto, Coherent structures and energy cascade in homogeneous turbulence, Prog. Theor. Phys. Suppl. **195**, 139 (2012).
[20] T. Leung, N. Swaminathan, and P. A. Davidson, Geometry and interaction of structures in homogeneous isotropic turbulence, J. Fluid Mech. **710**, 453 (2012).
[21] N. A. K. Doan, N. Swaminathan, P. A. Davidson, and M. Tanahashi, Scale locality of the energy cascade using real space quantities, Phys. Rev. Fluids **3**, 084601 (2018).
[22] S. Goto, Y. Saito, and G. Kawahara, Hierarchy of antiparallel vortex tubes in spatially periodic turbulence at high Reynolds numbers, Phys. Rev. Fluids **2**, 064603 (2017).
[23] M. Hirota, Y. Nishio, S. Izawa, and Y. Fukunishi, Hierarchical vortical structures extracted from turbulent fields, Fluid Dyn. Res. **52**, 015503 (2019).
[24] T. Yoneda, S. Goto, and T. Tsuruhashi, Mathematical reformulation of the Kolmogorov-Richardson energy cascade in terms of vortex stretching, Nonlinearity **35**, 1380 (2022).
[25] T. Tsuruhashi, S. Goto, S. Oka, and T. Yoneda, Self-similar hierarchy of coherent tubular vortices in turbulence, Phil. Trans. R. Soc. A. **380**, 20210053 (2022).
[26] C. Meneveau and T. S. Lund, On the Lagrangian nature of the turbulence energy cascade, Phys. Fluids **6**, 2820 (1994).
[27] J. I. Cardesa, A. Vela-Martín, S. Dong, and J. Jiménez, The temporal evolution of the energy flux across scales in homogeneous turbulence, Phys. Fluids **27**, 111702 (2015).
[28] J. I. Cardesa, A. Vela-Martín, and J. Jiménez, The turbulent cascade in five dimensions, Science **357**, 782 (2017).
[29] T. Makihara, S. Kida, and H. Miura, Automatic tracking of low-pressure vortex, J. Phys. Soc. Jpn. **71**, 1622 (2002).

[30] W. A. Kareem, S. Izawa, A. K. Xiong, and Y. Fukunishi, Extraction and tracking of multi-scaled vortices from a homogeneous isotropic turbulent field, J. Turbul. **8**, N12 (2007).

[31] A. Lozano-Durán and J. Jiménez, Time-resolved evolution of coherent structures in turbulent channels: Characterization of eddies and cascades, J. Fluid Mech. **759**, 432 (2014).

[32] E. Villermaux, B. Sixou, and Y. Gagne, Intense vortical structures in grid-generated turbulence, Phys. Fluids **7**, 2008 (1995).

[33] K. Alvelius, Random forcing of three-dimensional homogeneous turbulence, Phys. Fluids **11**, 1880 (1999).

[34] K. Yoshida, J. Yamaguchi, and Y. Kaneda, Regeneration of small eddies by data assimilation in turbulence, Phys. Rev. Lett. **94**, 014501 (2005).

[35] J. C. R. Hunt, A. A. Wray, and P. Moin, Eddies, streams, and convergence zones in turbulent flows, in *Studying Turbulence Using Numerical Simulation Databases, 2* (Center for Turbulence Research, Stanford University, California, USA, 1988), pp. 193–208.

[36] M. S. Chong, A. E. Perry, and B. J. Cantwell, A general classification of three-dimensional flow fields, Phys. Fluids A: Fluid Dyn. **2**, 765 (1990).

[37] J. Jeong and F. Hussain, On the identification of a vortex, J. Fluid Mech. **285**, 69 (1995).

[38] P. Chakraborty, S. Balachandar, and R. J. Adrian, On the relationships between local vortex identification schemes, J. Fluid Mech. **535**, 189 (2005).

[39] D. I. Pullin and Y. Yang, Whither vortex tubes? Fluid Dyn. Res. **46**, 061418 (2014).

[40] D. S. Pradeep and F. Hussain, Vortex dynamics of turbulence–coherent structure interaction, Theor. Comput. Fluid Dyn. **24**, 265 (2010).

[41] W. M. van Rees, F. Hussain, and P. Koumoutsakos, Vortex tube reconnection at Re = 104, Phys. Fluids **24**, 075105 (2012).

[42] R. M. Kerr, Swirling, turbulent vortex rings formed from a chain reaction of reconnection events, Phys. Fluids **25**, 065101 (2013).

[43] J. Yao and F. Hussain, Polarized vortex reconnection, J. Fluid Mech. **922**, A19 (2021).